JACS
JOURNAL OF THE AMERICAN CHEMICAL SOCIETY
Article
pubs.acs.org/JACS

Sterically Directed Functionalization of the Redox-Active Bis(imino)acenaphthene Ligand Class: An Experimental and Theoretical Investigation

Daniel A. Evans,[†] Ignacio Vargas-Baca,[‡] and Alan H. Cowley*[,†]

[†]Department of Chemistry and Biochemistry, The University of Texas at Austin, Austin, Texas 78712, United States
[‡]Department of Chemistry and Chemical Biology, McMaster University, Hamilton, Ontario, Canada L8S 4M1

Supporting Information

ABSTRACT: The synthesis, characterization, and theoretical study of the sterically directed functionalization of the redox-active bis(imino)acenaphthene (BIAN) ligand class has been explored. With dependence on the steric congestion encompassing the N−C−C−N fragment of the Ar-BIAN ligand, functionalization can be directed to proceed either via a radical backbone dearomatization or a nucleophilic imine C-alkylation pathway. The structures of the Ar-BIAN derivatives **14**−**19** were determined by means of single-crystal X-ray diffraction. The reaction pathways involved in Ar-BIAN functionalization were monitored by means of EPR spectroscopy. The experimental results and observations were examined in conjunction with DFT-D calculations in order to explain the driving forces that direct the pathways leading to Ar-BIAN functionalization.

INTRODUCTION

Sterically directed reactions represent a valuable method for performing organic transformations that involve the control of regioselectivity. The use of such steric effects can result in the availability of reaction pathways that would otherwise be dominated by electronic effects.[1] As an example, electrophilic aromatic substitution is typically dominated by electronic effects, which fall in two distinct categories, namely ortho−para directors and meta directors. However, it has been demonstrated that such reactions can be significantly influenced by means of steric effects. Such sterically directed reactions have been found to be useful in the contexts of, for example, the conjugate addition of unsaturated esters,[2] the synthesis of oxindole-fused spirooxirane and spirodihydrofuran compounds,[3] as well as the syntheses of Boc-protected 4-alkylprolinols and prolines.[4] The present work is devoted to a detailed study of the sterically directed functionalization of the redox-active bis(imino)acenaphthene (BIAN) ligand class.

Recently, the dpp-BIAN ligand (**1**) (dpp = 2,6-diisopropylphenyl) has been functionalized by treatment with a variety of nucleophiles, the outcomes of which are summarized in Figure 1. The first such reaction of this type was reported by Fedushkin et al.[5] and resulted in formation of a novel chiral *n*-butylated amido-imine lithium BIAN* complex (**2**) (BIAN* = amido-imine BIAN). A consequence of adopting the direct imine C-alkylation pathway is preservation of the backbone aromaticity of the functionalized BIAN* molecule. Subsequently, this approach has been extended to include the use of group 13 alkyl reagents for the syntheses of three additional BIAN* complexes (**3**, **4**, and **5**) (Figure 1).[6]

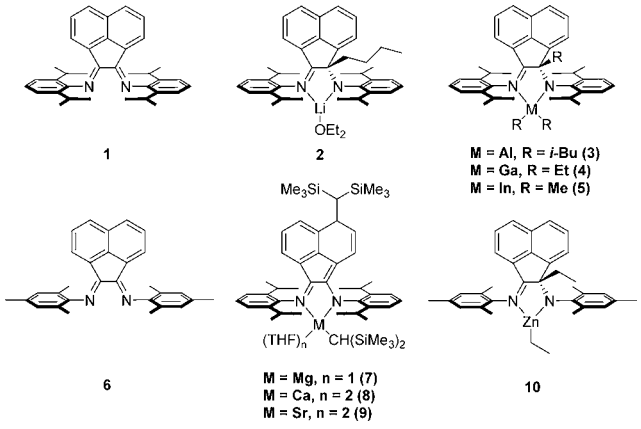

Figure 1. Functionalization of the Ar-BIAN Ligand Class.

In contrast to the work of Fedushkin et al.,[5] a study performed by Hill et al.[7] revealed that the reaction of dpp-BIAN with the bulky nucleophile K[CH(SiMe$_3$)$_2$] resulted in the formation of a backbone dearomatized derivative of BIAN*. In this interesting reaction, the [CH(SiMe$_3$)$_2$]$^-$ anion functionalized the backbone of the dpp-BIAN molecule, thereby dearomatizing one of the naphthalene rings and generating a different chiral BIAN* complex. This process can also be carried out by treatment of dpp-BIAN with metal complexes of

Received: July 10, 2013
Published: August 19, 2013

   dx.doi.org/10.1021/ja407070y | J. Am. Chem. Soc. 2013, 135, 13939−13946

the general type M[(CH(SiMe$_3$)$_2$)$_2$(THF)$_n$] (Figure 1) (**7**, **8**, and **9**).

Subsequently, Dagorne and Avilés et al.[8] treated the less sterically encumbered 2,4,6-trimethylphenyl (mes) BIAN (**6**) with diethyl zinc, thereby forming a mes-substituted ethyl BIAN* zinc complex (**10**). The latter mes-BIAN* zinc complex was found to be similar to that reported earlier by Fedushkin et al.[6]

In previously published work, we have described the outcome of the reaction of dpp-BIAN with *t*-butyllithium (*t*-BuLi), as displayed in Scheme 1.[9] The product of this reaction

Scheme 1. Reaction of dpp-BIAN with *t*-Butyllithium

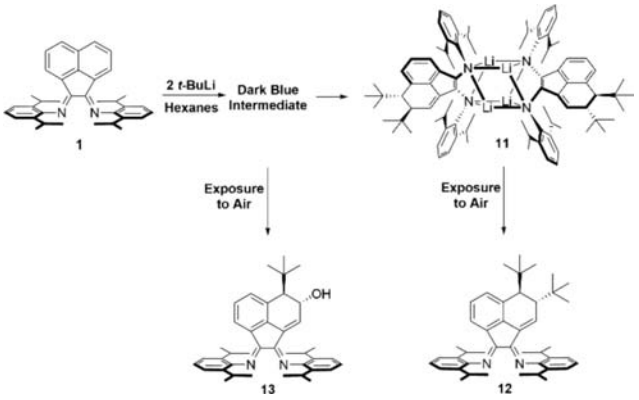

was completely unanticipated and featured the formation of an unprecedented vicinal *t*-butylated, dearomatized Li-BIAN antiprismatic complex (**11**) that differed significantly from any of the previous compounds presented in Figure 1. Exposure of **11** to air resulted in the formation of the oxidized free diimine dearomatized BIAN compound (**12**). Prompt hydrolysis of the transient blue-colored intermediate solution that had been formed in the course of this reaction generated the vicinal *t*-butyl-hydroxyl BIAN derivative (**13**). EPR analysis of the aforementioned blue-colored intermediate solution confirmed the radical nature of this unique dearomatization reaction (Figure 5).[9]

The radical dearomatization of dpp-BIAN that occurred following treatment with *t*-BuLi was both a fascinating and unexpected result that in turn posed several synthetic and mechanistic questions. First, what is the thermodynamic driving force behind the BIAN functionalization referred to above? A further question is related to the possibility of controlling and explaining the regioselectivity of each of the foregoing reactions. The final question concerns the possibility of synthesizing a *t*-butylated BIAN* ligand. Alternatively, does *t*-BuLi prefer to adopt an exclusive radical dearomatization pathway? The overall objective of the present work was to perform a comprehensive investigation of the reactions of the BIAN ligand class with a selection of bulky alkyllithium reagents.

RESULTS AND DISCUSSION

Syntheses of 14−19. A survey of the pertinent BIAN literature revealed that thus far, the majority of the chemistry of this ligand has been carried out using the sterically demanding 2,6-diisopropylphenyl (dpp) group as the nitrogen substituent. As a result, interest was generated in investigating the consequences of using nitrogen substituents with more modest steric bulk.

As mentioned earlier, the outcome of the reaction of dpp-BIAN with *t*-BuLi has been explored previously.[9] As might be anticipated on the basis of steric bulk, the 2,4,6-trimethylphenyl (mes) BIAN ligand, while slightly less sterically encumbered than the dpp-BIAN ligand, was predicted to behave in a similar fashion to the latter. On the other hand, the flanking imino aryl groups of the 4-fluorophenyl (4-F) and 4-methoxyphenyl (4-MeO) derivatives were selected because they exhibit opposite polarities and provide less steric protection of the N−C−C−N fragment of the BIAN ligand in comparison with their dpp-BIAN and mes-BIAN counterparts.

The first such reaction of this genre to be explored was that of mes-BIAN with *t*-BuLi. For this purpose, a red toluene solution of mes-BIAN was treated with *t*-BuLi, thereby

Scheme 2. Scope of Ar-BIAN Functionalization

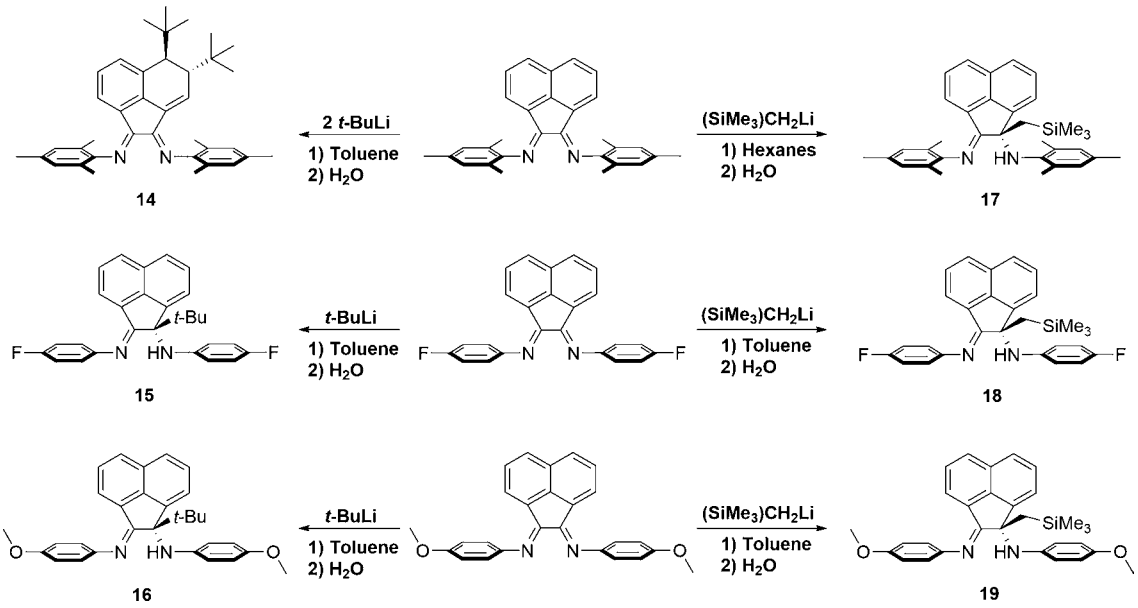

dx.doi.org/10.1021/ja407070y | J. Am. Chem. Soc. 2013, 135, 13939−13946

producing a dark green solution that gradually became deep purple over a period of several hours. After 48 h, exposure of the purple solution to air resulted in a slow color change of the reaction mixture from purple to dark red. Following concentration of the dark red toluene solution, the crude product was purified and recrystallized resulting in the formation of a crop of large red crystals of **14**. The structure of **14**, which was confirmed by means of single-crystal X-ray diffraction, was found to be that of a vicinal *t*-butylated, backbone dearomatized BIAN compound analogous to the one obtained previously by treatment of *t*-BuLi with dpp-BIAN (**12**).

The foregoing result was of significant interest because it proved that dearomatization of the BIAN ligand was not confined to dpp-BIAN. In subsequent work, the effects of using less bulky 4-F- and 4-MeO-substituted BIAN compounds were explored, in order to determine whether further reduction in ligand size and changes in ligand polarities would have an impact on their reactivities toward *t*-BuLi.

Treatment of toluene solutions of the 4-F- and 4-MeO-substituted BIAN compounds with *t*-BuLi resulted in immediate color changes of the reaction mixtures from orange to dark purple-brown and red to dark green-yellow, respectively. Over time, the above reaction mixtures gradually assumed dark yellow (4-F) and dark green hues (4-MeO). Hydrolysis of both of the foregoing reaction mixtures resulted in color changes from dark yellow to amber and from dark green to dark red-brown, respectively, thereby generating compounds **15** (4-F) and **16** (4-MeO).

The above compounds were purified and recrystallized, resulting in two crops of X-ray quality crystals. The structures of both compounds were determined by means of single-crystal X-ray diffraction, which confirmed their identities to be those of the *t*-butylated BIAN* derivatives **15** (4-F) and **16** (4-MeO). Surprisingly, the structures of both compounds were quite distinct from those of the vicinal *t*-butylated, backbone dearomatized products that had been isolated from the corresponding reactions of dpp-BIAN and mes-BIAN with *t*-BuLi, which resulted in compounds **12** and **14**, respectively.

Interestingly, the mode of attack of *t*-BuLi on the BIAN ligand is particularly sensitive to the nature of the flanking aryl groups of the BIAN moiety. In order to learn more about this unanticipated behavior of *t*-BuLi, the reactivity of a comparable sterically demanding alkyllithium reagent was explored.

In an elegant study by Kiplinger et al.,[10] it was discovered that the bulky $\{[(SiMe_3)CH_2]_3(THF)_2Lu\}$ complex was able to transfer a (trimethylsilyl)methyl group and thus dearomatize one of the pyridine rings of the terpy (2,2′:6′,2″-terpyridine) ligand. Inspired by this study, we decided to explore the reactions of (trimethylsilyl)methyllithium (TMS−CH_2−Li) with a selection of Ar-BIAN compounds.

Treatment of a red hexanes solution of mes-BIAN with TMS−CH_2−Li resulted in the development of a dark amber-brown solution that retained its color over a period of several hours. Following hydrolysis, the amber-brown solution assumed an orange-yellow hue, and the resulting product was extracted into a hexanes solution. Recrystallization via slow evaporation of the latter hexanes solution resulted in the formation of a crop of yellow-brown crystals. On the basis of a single-crystal X-ray diffraction study, the identity of the product was found to be that of the (trimethylsilyl)methyl amino-imine mes-BIAN* compound (**17**). Interestingly, the outcomes of the reactions of mes-BIAN with two comparably large alkyllithium reagents resulted in the formation of two distinctly different BIAN derivatives (**14** and **17**) (Figure 2).

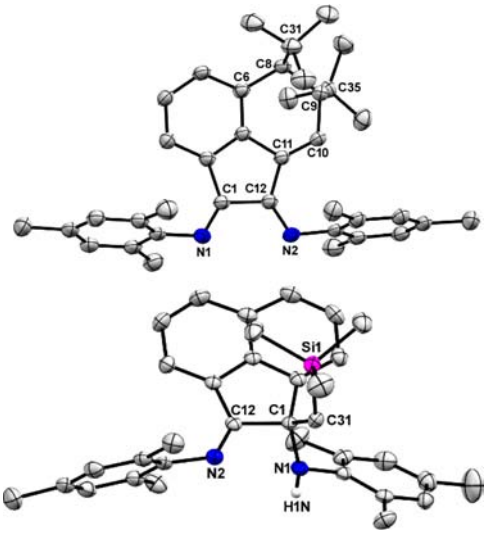

Figure 2. POV-Ray diagrams of **14** (upper) and **17** (lower) with thermal ellipsoids displayed at 50% probability. All hydrogen atoms have been removed for clarity with the exception of the amino hydrogen. Compound **14** crystallized with two independent molecules in the asymmetric unit, only one of which is displayed for clarity.

Treatment of toluene solutions of the 4-F- and 4-MeO-substituted BIAN compounds with TMS−CH_2−Li, resulted in color changes of the reaction mixtures from orange to purple-red and from red to dark purple, respectively. Furthermore, over time the 4-F and 4-MeO reaction mixtures slowly assumed a bright red and a dark red-brown color, respectively. Hydrolysis of these reaction mixtures resulted in the formation of a dark yellow solution (4-F) and a light red-orange solution (4-MeO). Concentration of these toluene solutions, followed by purification and subsequent recrystallization, resulted in the formation of crystals of both compounds that were suitable for single-crystal X-ray diffraction studies. The resulting structural data confirmed the identities of these compounds to be the (trimethylsilyl)methyl-substituted BIAN* compounds **18** (4-F) and **19** (4-MeO) akin to that of the (trimethylsilyl)methyl mes-BIAN* compound (**17**).

Characterization of 14−19. Compounds **14−19** were characterized by means of ^{1}H, ^{13}C, ^{19}F NMR, mass spectrometry, and single-crystal X-ray diffraction. The pertinent ^{1}H, ^{13}C, and ^{19}F NMR and mass spectrometric data can be found in the Supporting Information.

Single-Crystal X-ray Diffraction Studies. Compounds **14−19** were structurally characterized by means of single-crystal X-ray diffraction. Pertinent bond lengths and angles are listed in Table 1 and complete X-ray crystallographic data are available in the Supporting Information.

Compound **14** crystallized with two independent molecules in the asymmetric unit (Figure 2). The N−C−C−N fragment of compound **14** retained its diimine functionality following treatment with *t*-BuLi and subsequent oxidation in air, as indicated by the resulting average C═N bond length of 1.277 (2) Å. The backbone of **14** was dearomatized as a consequence of vicinal *t*-butylation at C(8), C(9), C(46), and C(47). The four carbon fragments that contain the units C(6)−C(8)−C(9)−C(10) and C(44)−C(46)−C(47)−C(48) were both

dx.doi.org/10.1021/ja407070y | J. Am. Chem. Soc. 2013, 135, 13939−13946

Table 1. Selected Bond Lengths (Å) and Bond Angles (°) for 15−19

	15	16	17	18a	18b	19
bond lengths (Å)						
N(1)−C(1)	1.465(3)	1.486(4)	1.501(3)	1.450(3)	1.456(3)	1.454(3)
C(1)−C(12)	1.564(3)	1.564(5)	1.557(3)	1.558(3)	1.567(3)	1.562(4)
C(12)−N(2)	1.270(3)	1.278(4)	1.272(3)	1.273(3)	1.280(3)	1.268(3)
bond angles (°)						
C(1)−N(1)−H(1N)	109.7(17)	111(2)	108.3(16)	111.7(18)	112.6(16)	112(2)
N(1)−C(1)−C(12)	112.65(18)	112.3(3)	103.73(16)	114.16(17)	112.57(16)	112.2(2)
N(2)−C(12)−C(1)	119.5(2)	119.3(3)	118.80(19)	119.85(17)	119.54(17)	120.1(2)

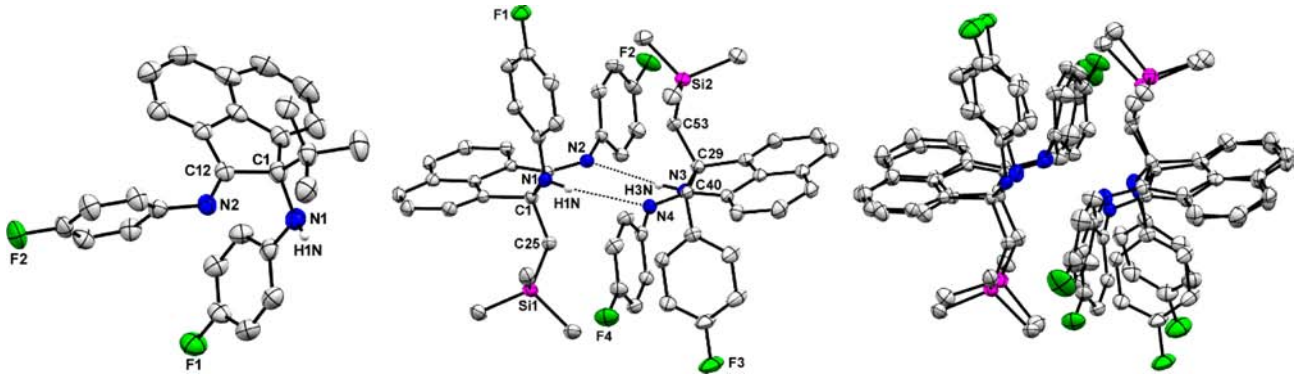

Figure 3. POV-Ray diagrams of **15** (left), **18a** (center), and the overlaid diagram for polymorphs **18a** and **18b** (right) with thermal ellipsoids displayed at 50% probability. All hydrogen atoms were removed for clarity with the exception of the amino hydrogen.

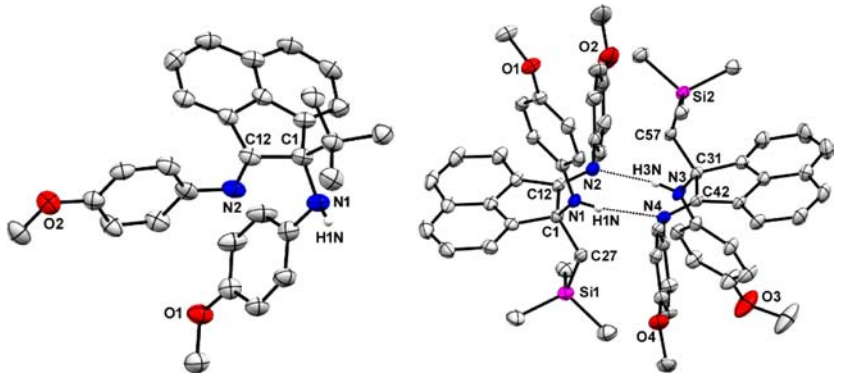

Figure 4. POV-Ray diagrams of **16** (left) and **19** (right) with thermal ellipsoids displayed at 50% probability. All hydrogen atoms were removed for clarity with the exception of the amino hydrogen.

dearomatized as evidenced by the average C−C bond length of 1.531 (3) Å. Note that a localized double bond is retained between C(10)−C(11) and C(48)−C(49), as indicated by the average C═C bond length of 1.331 (3) (Å). The average torsion angle between the vicinal *t*-butyl groups is 142.60 (18) degrees. Finally, as a consequence of vicinal *t*-butylation, chiral centers were generated at C(8), C(9), C(46), and C(47). However, this transformation occurred with high stereoselectivity and resulted in the exclusive formation of the trans stereoisomer.

Compounds **15** and **16** both crystallized with one molecule in the asymmetric unit (Figures 3 and 4). Inspection of the metrical parameters for the N−C−C−N fragments of **15** and **16** revealed that imine *t*-butylation of these compounds resulted in the formation of BIAN* derivatives. Interestingly, compounds **15** and **16** do not exhibit intermolecular hydrogen-bonding interactions within their crystal lattices, despite the fact that both N−C−C−N fragments feature a hydrogen bond donor amino group and a hydrogen bond acceptor imine moiety. The absence of these favorable hydrogen-bonding interactions from the packing of the crystal lattice emphasizes the highly sterically encumbered nature of the *t*-butylated N−C−C−N fragment.

Compound **17** crystallized with one molecule in the asymmetric unit and is structurally similar to **15** and **16** (Figure 2). Akin to **15** and **16**, compound **17** does not exhibit intermolecular hydrogen-bonding interactions within the crystal lattice. This observation indicates that, although the TMS−CH_2 group is slightly less sterically demanding than a *t*-butyl group, the steric environment encompassing the N−C−C−N fragment remains congested due to the presence of methyl groups located at the 2 and 6 positions of the flanking aryl group of the mes substituent.

Compounds **18a** and **19** both crystallized with two molecules in their respective asymmetric units. Both molecules exist as hydrogen-bound dimers, as evident in Figures 3 and 4. This

dx.doi.org/10.1021/ja407070y | J. Am. Chem. Soc. 2013, 135, 13939−13946

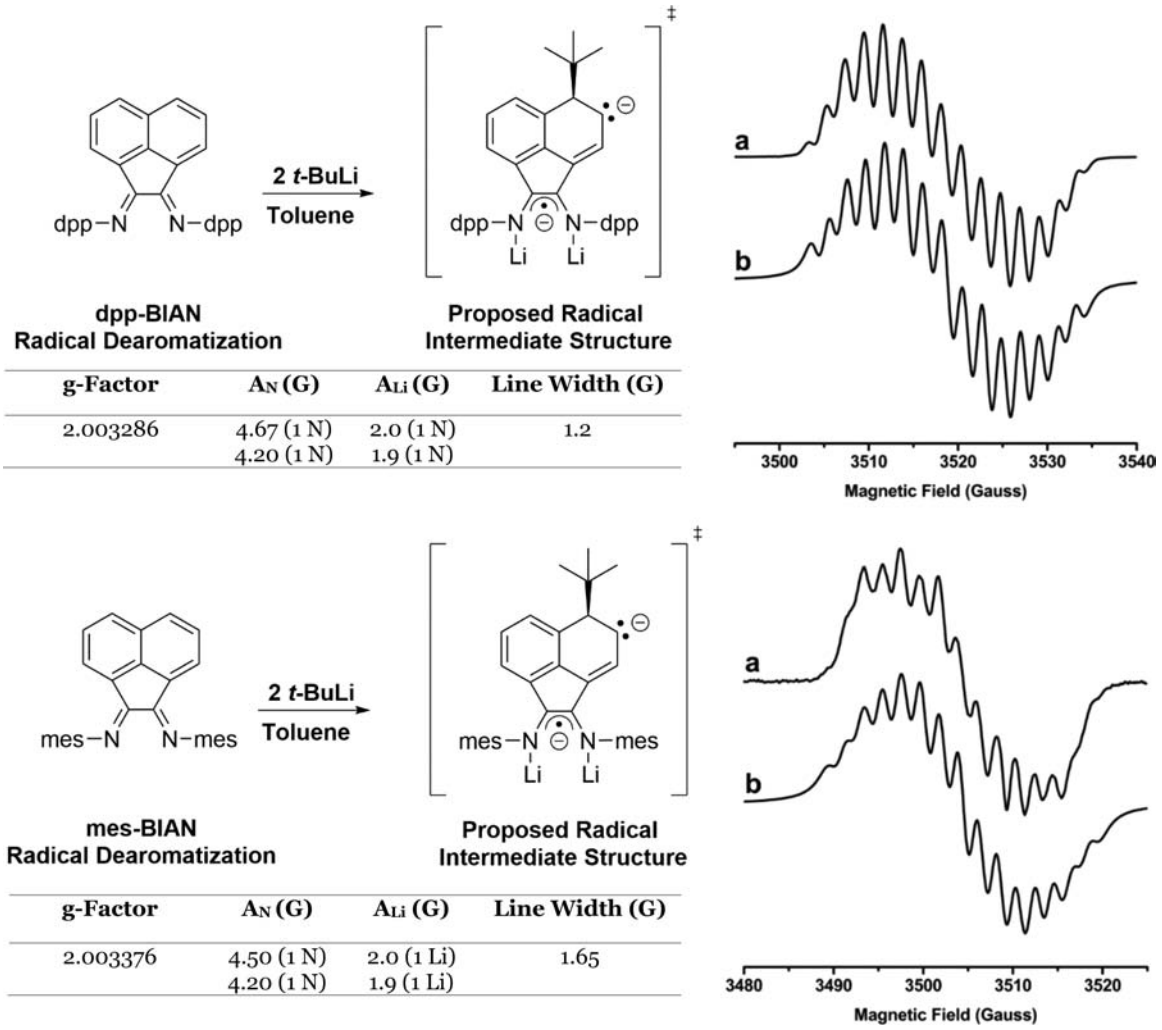

g-Factor	A_N (G)	A_{Li} (G)	Line Width (G)
2.003286	4.67 (1 N) 4.20 (1 N)	2.0 (1 N) 1.9 (1 N)	1.2

g-Factor	A_N (G)	A_{Li} (G)	Line Width (G)
2.003376	4.50 (1 N) 4.20 (1 N)	2.0 (1 Li) 1.9 (1 Li)	1.65

Figure 5. X-band (9.87 GHz) EPR spectra of the radical intermediates of the reaction of *t*-BuLi with dpp-BIAN (top) and *t*-BuLi with mes-BIAN (bottom). Both spectra were recorded in toluene solution at room temperature: (a) experimental spectra; (b) simulated spectra.

favorable type of hydrogen-bonded crystal packing demonstrates that the steric encumbrance of the N−C−C−N fragment is diminished in compounds **18a** and **19**. Moreover, there is a clear distinction between the structures of compounds **15** and **16** and compounds **18a** and **19** in terms of intermolecular hydrogen-bonding interactions. All four crystal structures have the potential to crystallize as hydrogen-bound dimers. However, this type of dimerization is only observed in the cases of compounds **18a** and **19**. The foregoing distinction highlights the differences in the steric characteristics of the two bulky nucleophiles that were employed in the present work.

Interestingly, the recrystallization of **18** resulted in the formation of two polymorphs within the same recrystallization vial (**18a** and **18b**). Compound **18a** crystallized with two molecules in the asymmetric unit, while **18b** crystallized with only one such molecule in the asymmetric unit. Inspection of the crystal packing diagram for **18b** confirmed the anticipated formation of a hydrogen-bound dimer across an inversion center analogous to those found for **18a**. A superimposed diagram of the polymorphs **18a** and **18b** was generated in order to display how these structures differ with respect to orientation (Figure 3).

EPR Spectroscopic Studies. As mentioned earlier, it was determined that the reaction of dpp-BIAN with *t*-BuLi did not proceed via a traditional nucleophilic dearomatization process[11] but instead underwent radical dearomatization.[9] This conclusion was reached on the basis of an EPR analysis of the reaction intermediate of dpp-BIAN with *t*-BuLi (Figure 5). The pertinent EPR spectrum, which is presented in Figure 5, exhibits a 15-lined spectrum due to hyperfine coupling of the unpaired electron with two nonequivalent ^{14}N nuclei (I = 1, natural abundance 99.6%) and two nonequivalent ^{7}Li nuclei (I = 3/2, natural abundance 92.58%). (The hyperfine coupling of an unpaired electron to the N−C−C−N fragment of BIAN radical anions is well-known).[12] The radical intermediate structure was proposed on the basis of hyperfine coupling in conjunction with the X-ray crystal structure analysis of compound **13**. The presence of nonequivalent hyperfine coupling constants can be explained on the basis of breaking the C_{2v} symmetry via mono *t*-butylation, as confirmed by the structure of the mono *t*-butylated-hydroxyl BIAN derivative (**13**). The existence of hyperfine coupling between two nonequivalent nitrogen and two nonequivalent lithium nuclei resulted in the proposed $[Li]_2[t\text{-Bu-dpp-BIAN}]$ radical intermediate structure that is displayed in Figure 5.

Given the foregoing, it was proposed that the formation of the analogous vicinal *t*-butylated, backbone dearomatized mes-BIAN compound would proceed via a similar radical

dx.doi.org/10.1021/ja407070y | J. Am. Chem. Soc. 2013, 135, 13939−13946

Scheme 3. Competing Pathways for the Reactions of Ar-BIAN and Organolithium Reagents

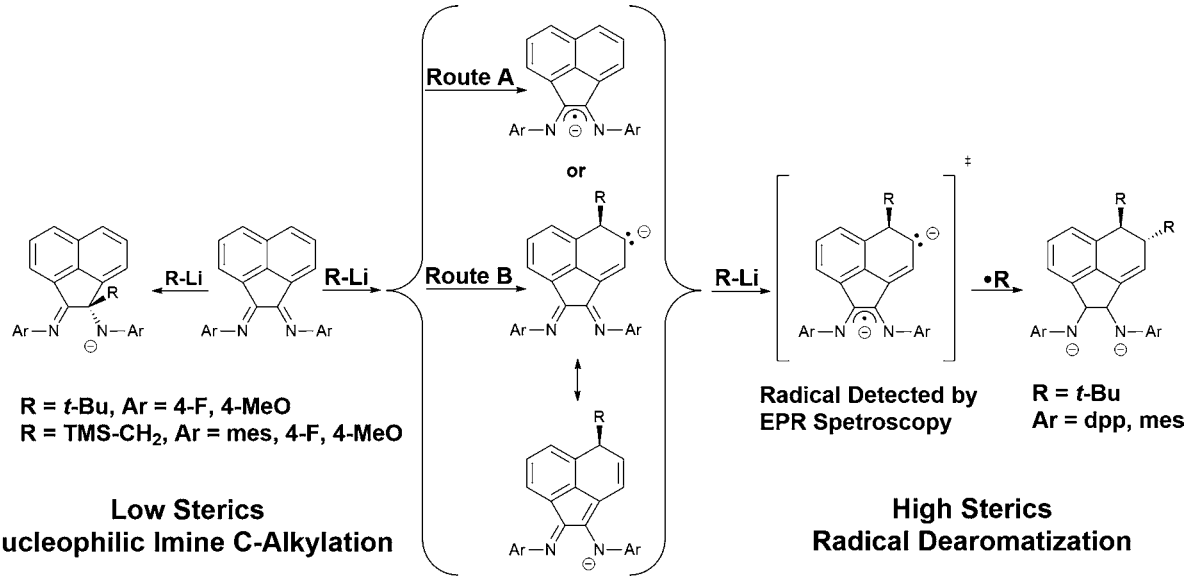

dearomatization pathway. In order to confirm this hypothesis, the dark-green intermediate solution, which had been generated during the reaction of mes-BIAN with *t*-BuLi in toluene solution, was analyzed by means of EPR spectroscopy. As evident from Figure 5, the EPR spectrum that was recorded for the reaction intermediate of mes-BIAN exhibits a similar hyperfine structure to that observed for dpp-BIAN. The EPR spectrum in question, which is presented in Figure 5, features a somewhat broadened 15-lined hyperfine structure on account of the hyperfine coupling of the unpaired electron to two nonequivalent ^{14}N nuclei and two nonequivalent ^{7}Li nuclei. The proposed radical intermediate structure presented in Figure 5 corresponds to that of a mono-*t*-butylated dilithium radical structure akin to the one proposed for dpp-BIAN. The parallels between the radical intermediate structures of mes-BIAN and dpp-BIAN with respect to their reactivities with *t*-BuLi were anticipated on the basis of steric bulk and X-ray structure analysis of **12** and **14**.

Computational Modeling. As mentioned earlier, a significant difference in reactivity of mes-BIAN was observed upon changing the incoming nucleophile from *t*-Bu to TMS-CH_2, the net result of which was that nucleophilic imine C-alkylation occurred rather than radical backbone dearomatization. In turn, this observation raised an important mechanistic question, namely, what dictates the pathway of Ar-BIAN functionalization? Accordingly, DFT calculations were employed in order to assess the relevance of the factors that could govern the competition between imine C-alkylation and dearomatization of the naphthalene ring system when Ar-BIAN molecules were allowed to react with organolithium reagents. As demonstrated by EPR spectroscopy, the formation of the radical dianion (coordinated to lithium) represents a key stage along the dearomatization pathway. The generation of such a species would take place along one of two alternative two-stage pathways (Scheme 3): routes A and B. Route A: electron transfer from R-Li to Ar-BIAN, followed by nucleophilic addition of the second equivalent of R-Li. Route B: nucleophilic addition of R^-, followed by electron transfer from R-Li. The transient monoanion would be resonance stabilized.

Both of the above routes imply formation of the •R free radical, which would be more easily generated from *t*-BuLi than from *n*-BuLi or TMS-CH_2-Li. Such a radical would couple to the radical anion, thereby forming the dialkylated dianion as evident in the structure of **11.**

In the interest of expedience, all calculations were carried out at the level of the General Gradient Approximation using the Perdew–Burke–Ernzerhof[13] (PBE) functional supplemented with Grimme's D3[14] dispersion correction, in order to account properly for steric effects.

The calculations for the models of Ph-BIAN, 4-F-BIAN, and 4-MeO-BIAN included geometry optimizations and vibrational calculations of their neutral and reduced monoanions from which the respective adiabatic zero-point, energy-corrected electron affinities were determined to be −165.6, −152.3, and −139.3 kJ/mol, respectively. The foregoing exothermic values are consistent with the well-known electron acceptor ability of the BIAN ligand family and follow the trends expected on the basis of the nature of the substituent groups on the phenyl ring.[15]

The same calculations permit identification of the reactive sites of the molecule with respect to the addition of a nucleophile using the integrated-from-above Fukui function,[16,17] $f^+(r)$ in eq 1. This property can be visualized as a projection of the density change upon one-electron addition to the LUMO onto the electron density. Maps of the electrophilic regions of Ph-BIAN and its reduced monoanion radical are presented in Figure 6.

$$f^+(r) = \rho(r)_{1-} - \rho(r)_1 \quad (1)$$

The Fukui function plot clearly indicates that the site for a nucleophilic attack on Ph-BIAN takes place at the imino carbon atoms. This conclusion represents the primary reason why the reaction of organolithium reagents with Ar-BIAN compounds results in nucleophilic imine C-alkylation with the less bulky aryl substituents. On the other hand, the map for the radical $[Ph\text{-}BIAN]^-$ reveals that the reactive sites are naphthalenic carbons that are located primarily at position 5 and at the positions ipso to the diazabutadiene moiety. Positions 3 and 4 are less reactive than position 5 but cannot be disregarded

dx.doi.org/10.1021/ja407070y | J. Am. Chem. Soc. 2013, 135, 13939−13946

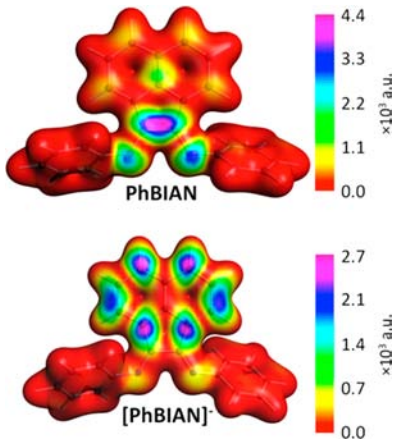

Figure 6. Fukui functions for nucleophilic attack mapped on the density isosurfaces (0.22 au) of Ph-BIAN (upper) and [Ph-BIAN]$^-$ (lower).

solely on these grounds. The same reactivity would be observed when the LUMO of Ar-BIAN is inaccessible due to steric protection by the substituents on the phenyl rings.

The relative stabilities of all possible isomers of the radical dianion [Ph-BIAN-R]$^{2-}$ that result from the attachment of R$^-$ to [Ph-BIAN]$^-$ were calculated from the corresponding total bonding energies that were obtained on the basis of the geometry optimizations for *R* = Me. For comparison and in order to consider an alternative pathway by which Ph-BIAN would initially undergo nucleophilic attack, calculations were also performed on [Ph-BIAN-Me]$^-$. The results obtained for all of these models and their 4-F and 4-MeO analogues are presented in Figure 7. (The resulting isomers are identified numerically according the IUPAC recommendation for acenaphthylene (Scheme 4)).

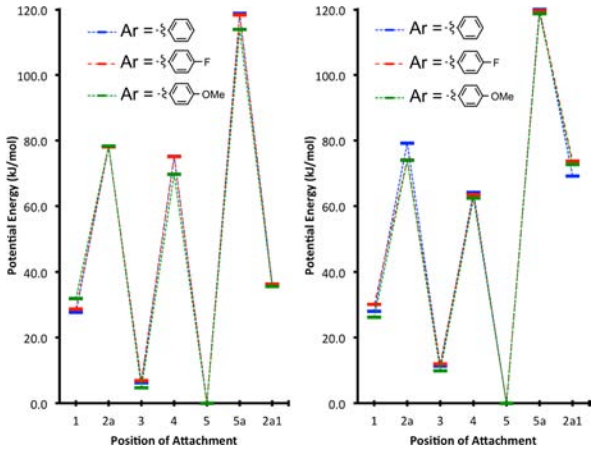

Figure 7. Relative stabilities of the isomers of [Ph-BIAN-Me]$^-$ (left) and [Ph-BIAN-Me]$^{2-}$ (right). (The plotted values have not been corrected for differences in zero point energy.)

The stability plots for [Ph-BIAN-Me]$^-$ and [Ph-BIAN-Me]$^{2-}$ are remarkably similar. In both instances, there is a thermodynamic preference for attachment of the methyl group at position 5 in agreement with the experimental EPR spectra in conjunction with the X-ray crystal structure of **13**. Moreover, in both cases, the binding at positions 2a, 4, and 5a would be energetically unfavorable. Although position 2a^1 is more accessible in the case of [Ph-BIAN-Me]$^-$ than [Ph-BIAN-Me]$^{2-}$, the Fukui maps eliminate this possibility. Furthermore, the Fukui maps discount any binding at position 3 for [Ph-BIAN-Me]$^-$, which puts this site at a disadvantage with respect to position 5 in [Ph-BIAN-Me]$^{2-}$. It is also noteworthy that despite the effect that the 4-F and 4-MeO substituents have on the electron affinity of the BIAN molecule, there is no meaningful influence on the stabilities of the alkylated derivatives.

Scheme 4. Labels Used to Identify the Potential Positions of Attachment of Alkyl Groups on Ar-BIAN

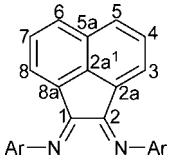

Interestingly, the products of attachment at position 1 of Ph-BIAN (the imino carbon) are 27.8 and 28.1 kJ/mol less stable than the preferred structures of the mono- and dianion, respectively. While the Fukui function for Ph-BIAN does provide a kinetic rationale for the nucleophilic imine C-alkylation reaction, the thermodynamic barrier for this process would be alleviated by chelation of the cation. This chelation factor was approximated by calculation of the energies of the isomers of the anion in the presence of a unitary point charge placed equidistantly at 2.0 Å from each nitrogen atom (the typical Li—N distance in BIAN derivatives) and within the average plane defined by the imino carbons. Although these calculations are obviously crude models, the difference in energy between the structures of the 1-substituted and 5-substituted isomers decreased by 14.8 kJ/mol. The other geometries were destabilized by as much as 32.9 kJ/mol, with the exception of the 2a^1-bound isomer, which became 13.4 kJ/mol more stable. Similarly, the calculated electron affinities of all the [Ar-BIAN-Me]$^-$ isomers are largely endothermic (>150 kJ/mol), which makes the pathway that includes electron transfer following nucleophilic attack less likely. However, this effect could be attenuated by chelation of the metal ion.

This aforementioned pathway (route B) is reminiscent of the work of Hill et al.,[7] which resulted in a single alkylation event accompanied by backbone dearomatization (Figure 1). However, this particular species was in fact the final product and not an intermediate. In view of the foregoing, the more likely reaction pathway is route A, which comprises an electron transfer process followed by the nucleophilic addition of R$^-$ at C(5).

As discussed above, bulky ortho-substituents can influence the reaction pathway by blocking access to the imino carbon atom. In addition to the kinetic factor, the size of the *t*-butyl group may be sufficient to destabilize the 1-substituted isomers of [Ph-BIAN-*t*-Bu]$^-$ and [Ph-BIAN-*t*-Bu]$^{2-}$. Surprisingly, the corresponding calculations for the 1-substituted isomer and the six remaining isomers revealed that the potential energy gaps actually decreased by 10.4 and 8.4 kJ/mol for the monoanion and dianion, respectively. Moreover, these values are comparable to the dispersion contributions to the stabilizing effect (9.3 and 8.4 kJ/mol).

The compositions of the SOMOs were derived on the basis of the calculations for the [Ph-BIAN-Me]$^{2-}$ models (Figure 8). With the exception of the product of imine C-alkylation, all the calculated radicals feature the delocalization of spin over the two nitrogen atoms. Of special interest is the electronic

dx.doi.org/10.1021/ja407070y | J. Am. Chem. Soc. 2013, 135, 13939−13946

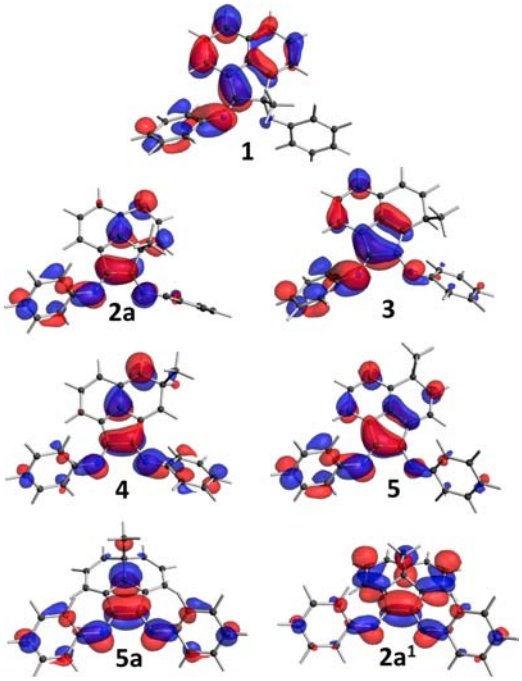

Figure 8. SOMOs (0.03 isosurfaces) of the isomers of $[Ph\text{-}BIAN\text{-}Me]^{2-}$. The structures are labeled according to the position of attachment of the methyl group.

structure of the 5-isomer, for which the small differences in Mulliken spin densities of the nitrogen atoms, 0.33 and 0.37, is consistent with the relative magnitudes of the experimental hyperfine coupling constants.

CONCLUSIONS

In conclusion, the present work describes the sterically directed functionalization of the redox-active Ar-BIAN ligand class. By tuning the steric bulk of the flanking aryl substituents, the pathways for nucleophilic imine C-alkylation and radical backbone dearomatization can be differentiated and controlled. The two reaction pathways discussed earlier were investigated on the basis of single-crystal X-ray diffraction studies, EPR spectroscopy, and computational modeling. Overall, it was determined that nucleophilic imine C-alkylation is the preferred pathway if the nucleophile can gain access to the electrophilic imino carbon, thus resulting in the formation of products **15**–**19**. However, if steric congestion inhibits this reaction pathway, the proposed mechanism comprises initial reduction of the N–C–C–N fragment of Ar-BIAN, followed by nucleophilic attack of the naphthalenic carbon located at position 5. This radical dianion intermediate species was investigated by EPR spectroscopy. Finally, this aforementioned radical dianion intermediate couples to a •R free radical, thereby producing the vicinal alkylated, backbone dearomatized Ar-BIAN derivative.

ASSOCIATED CONTENT

Supporting Information

Full experimental data, spectroscopic characterization, and single-crystal X-ray crystallographic data. This material is available free of charge via the Internet at http://pubs.acs.org.

AUTHOR INFORMATION

Corresponding Author

*acowley@cm.utexas.edu

Notes

The authors declare no competing financial interest.

ACKNOWLEDGMENTS

The generous financial support provided by the Robert A. Welch Foundation (Grant F-0003) (A.H.C.) and the Natural Sciences and Engineering Research Council of Canada (I.V.-B.) is gratefully acknowledged. This work was made possible by access to the facilities of the Shared Hierarchical Academic Research Computing Network (SHARCNET: www.sharcnet.ca) and Compute/Calcul Canada.

REFERENCES

(1) Chotana, G. A.; Rak, M. A.; Smith, M. R., III *J. Am. Chem. Soc.* **2005**, *127*, 10539–10544.
(2) Cooke, M. P., Jr. *J. Org. Chem.* **1986**, *51*, 1637–1638.
(3) Basavaiah, D.; Badsara, S. S.; Sahu, B. C. *Chem.—Eur. J.* **2013**, *19*, 2961–2965.
(4) Del Valle, J. R.; Goodman, M. *J. Org. Chem.* **2003**, *68*, 3923–3931.
(5) Fedushkin, I. L.; Hummert, M.; Schumann, H. *Eur. J. Inorg. Chem.* **2006**, 3266–3273.
(6) Tishkina, A. N.; Lukoyanov, A. N.; Morozov, A. G.; Fukin, G. K.; Lyssenko, K. A.; Fedushkin, I. L. *Russ. Chem. Bull., Int. Ed.* **2009**, *58*, 2250–2257.
(7) Arrowsmith, M.; Hill, M. S.; Kociok-Köhn, G. *Organometallics* **2011**, *30*, 1291–1294.
(8) Romain, C.; Rosa, V.; Fliedel, C.; Bier, F.; Hild, F.; Welter, R.; Dagorne, S.; Avilés, T. *Dalton Trans.* **2012**, *41*, 3377–3379.
(9) Evans, D. A.; Cowley, A. H. *J. Am. Chem. Soc.* **2012**, *134*, 15672–15675.
(10) Jantunen, K. C.; Scott, B. L.; Hay, P. J.; Gordon, J. C.; Kiplinger, J. L. *J. Am. Chem. Soc.* **2006**, *128*, 6322–6323.
(11) López Ortiz, F.; Iglesias, M. J.; Fernández, I.; Andújar Sánchez, C. M.; Ruiz Gómez, G. *Chem. Rev.* **2007**, *107*, 1580–1691.
(12) Fedushkin, I. L.; Skatova, A. A.; Chudakova, V. A.; Cherkasov, V. K.; Fukin, G. K.; Lopatin, M. A. *Eur. J. Inorg. Chem.* **2004**, 388–393.
(13) Perdew, J. P.; Burke, K.; Ernzerhof, M. *Phys. Rev. Lett.* **1996**, *77*, 3865–3868.
(14) Grimme, S.; Antony, J.; Ehrlich, S.; Krieg, H. *J. Chem. Phys.* **2010**, *132*, 154104/1–154104/19.
(15) Fedushkin, I. L.; Skatova, A. A.; Chudakova, V. A.; Fukin, G. K *Angew. Chem., Int. Ed.* **2003**, *42*, 3294–3298.
(16) Parr, R. G.; Yang, W. *J. Am. Chem. Soc.* **1984**, *106*, 4049–4050.
(17) Yang, W.; Parr, R. G.; Pucci, R. *J. Chem. Phys.* **1984**, *81*, 2862–2863.